

**One-neutron removal reactions on Al isotopes around the  $N = 20$  shell closure**

C. Nociforo,<sup>1</sup> A. Prochazka,<sup>1,2</sup> R. Kanungo,<sup>3</sup> T. Aumann,<sup>1</sup> D. Boutin,<sup>2</sup> D. Cortina-Gil,<sup>4</sup> B. Davids,<sup>5</sup> M. Diakaki,<sup>6</sup> F. Farinon,<sup>1,2</sup> H. Geissel,<sup>1,2</sup> R. Gernhäuser,<sup>7</sup> R. Janik,<sup>8</sup> B. Jonson,<sup>9</sup> B. Kindler,<sup>1</sup> R. Knöbel,<sup>1,2</sup> R. Krücken,<sup>7</sup> N. Kurz,<sup>1</sup> M. Lantz,<sup>9</sup> H. Lenske,<sup>2</sup> Yu. A. Litvinov,<sup>1</sup> B. Lommel,<sup>1</sup> K. Mahata,<sup>1</sup> P. Maierbeck,<sup>7</sup> A. Musumarra,<sup>10,11</sup> T. Nilsson,<sup>9</sup> C. Perro,<sup>3</sup> C. Scheidenberger,<sup>1,2</sup> B. Sitar,<sup>8</sup> P. Strmen,<sup>8</sup> B. Sun,<sup>2</sup> I. Szarka,<sup>8</sup> I. Tanihata,<sup>12</sup> H. Weick,<sup>1</sup> and M. Winkler<sup>1</sup>

<sup>1</sup>*GSI Helmholtzzentrum für Schwerionenforschung, D-64291 Darmstadt, Germany*

<sup>2</sup>*Justus-Liebig Universität Gießen, D-35392 Gießen, Germany*

<sup>3</sup>*Astronomy and Physics Department, Saint Mary's University, Halifax, NS B3H 3C3, Canada*

<sup>4</sup>*Universidade de Santiago de Compostela, E-15782 Santiago de Compostela, Spain*

<sup>5</sup>*TRIUMF, Vancouver, British Columbia V6T 2A3, Canada*

<sup>6</sup>*National Technical University, Athens, Greece*

<sup>7</sup>*Physik Department E12, Technische Universität München, D-85748 Garching, Germany*

<sup>8</sup>*Faculty of Mathematics and Physics, Comenius University, 84215 Bratislava, Slovakia*

<sup>9</sup>*Chalmers University of Technology, SE 412-916 Göteborg, Sweden*

<sup>10</sup>*INFN-LNS, I-95153 Catania, Italy*

<sup>11</sup>*University of Catania, I-95153 Catania, Italy*

<sup>12</sup>*RCNP, Osaka University, Mihogaoka, Ibaraki, Osaka 567 0047, Japan*

(Received 4 October 2011; revised manuscript received 17 February 2012; published 12 April 2012)

The one-neutron removal cross sections of neutron-rich Al isotopes and longitudinal momentum distributions of the residues have been measured for  $A = 33$  to  $36$  at relativistic energies ( $\approx 900$  MeV/u). The inclusive data have been interpreted within the eikonal approximation. The evolution of the single-particle occupancy in the ground state of <sup>33,34</sup>Al has been studied and compared with shell model predictions. The inferred  $2s_{1/2}$  neutron occupancy in the <sup>33</sup>Al ground-state wave function is 20% to 40% lower than the predicted one. The inclusive data do not exclude the presence of intruder states. Some intruder  $l = 1$  occupancy is found in <sup>34</sup>Al, similarly to <sup>33</sup>Mg. The single-particle  $1f_{7/2}$  occupancy shows a gradual increase at  $N = 22$ . Correspondingly, a decrease of the  $1d_{3/2}$  strength has been observed.

DOI: [10.1103/PhysRevC.85.044312](https://doi.org/10.1103/PhysRevC.85.044312)

PACS number(s): 25.60.Gc, 21.10.Jx, 21.60.Cs, 27.30.+t

**I. INTRODUCTION**

A highly interesting topic of modern nuclear structure research is to explore the evolution of the nuclear shell model far from the valley of  $\beta$  stability. The nuclear shell model, being so successful for stable nuclei, relies on the prevalence of a static nuclear potential and the dominance of mean-field dynamics. It is an open question as to what extent that concept is still valid in nuclei with large proton-neutron asymmetry. With this work we intend to contribute to this central question by an experimental study of neutron-rich Al isotopes in the mass region  $A = 33$  to  $36$ . The structure of nuclei in this region, commonly referred as the island of inversion [1], has been extensively studied since the seventies because of the anomalous breakdown of the  $N = 20$  shell closure observed initially in the Na and Mg isotopes [2,3]. In the case of Ne, Na, and Mg, a clear anomaly appears in the two-neutron separation energy ( $S_{2n}$ ) around  $N = 20$ , signaling shell closure breaking (see reviews [4,5]). On the other hand, the experimental  $S_{2n}$  of the Al isotopes do not show anomalies and are perfectly reproduced by large-scale shell model calculations involving the full  $sd$  proton shell and the  $pf$  neutron shell [6] as valence space.

Monte Carlo shell model calculations performed for the  $N = 20$  isotones with  $8 < Z < 20$  predict successfully the strengthening of the  $N = 20$  gap with increasing proton number [7]. However, a direct measurement of the weakness of the  $N = 20$  shell closure appears very difficult at lower  $Z$  (e.g., <sup>28</sup>O is particle unbound [8]). On the contrary, the neutron-rich

Al isotopes around  $N = 20$ , located in a transition region between the spherical shell of Si nuclei and the deformed Mg isotopes, are easier to access experimentally. The ground-state structure of <sup>33</sup>Al was first investigated by measuring the  $\beta$ -decay half-life and the  $\gamma$ -ray spectrum obtained from <sup>33</sup>Mg [9]. Comparisons between the experimental and theoretical  $\beta$  decay on one side and the  $\beta$ -delayed neutron-emission branching ratios on the other side left <sup>33</sup>Al outside the island of inversion [10]. Recent magnetic moment measurements performed on the <sup>33,34</sup>Al isotopes [11,12] have shown large discrepancies with shell model predictions in the  $sd$  and  $sdpf$  model spaces. Such discrepancies have been interpreted as an indication of the non-negligible presence of intruder configurations in the <sup>33</sup>Al and <sup>34</sup>Al ground-state wave functions. At  $N = 20$  and  $Z = 11, 12$  the experimental  $g$  factors were already found to deviate strongly from the  $sd$  shell model predictions. Particle-hole excitations recognized as intruder states have been also found in excited states of <sup>32</sup>Al at around 1 MeV and of <sup>33</sup>Al at 730 keV [13,14]. Thus, a possible extension of a deformed region beyond  $Z = 12$  has been considered.

The first spectroscopic study of nucleus <sup>33</sup>Ne has been reported, showing the extension of the island of inversion to at least  $N = 22$  for the Ne isotopes [15]. For the odd-mass Al isotopes ( $N = 20, 22$ ), information on the occupied orbitals of the unpaired neutron can be extracted on the basis of shell model predictions. Precise  $g$ -factor measurements were found to be very sensitive to the isospin and strongly influenced by the presence of intruder states. An admixture of at least

25% neutron  $2p$ - $2h$  intruder states has been suggested in the ground-state wave function of  $^{33}\text{Al}$  [11]. The measurement of the  $^{33}\text{Al}$  quadrupole moment has recently suggested a presence of intruder states at a level higher than 60% [16]. It was also suggested that the neutron occupancy of the  $2p_{3/2}$  orbital for the Mg isotopes is larger at  $N = 21$  than  $N = 20$  [17]. In order to achieve better agreement with the data, a lowering of the  $2p_{3/2}$  level by 1 MeV was proposed.

For the even-mass Al isotopes ( $N = 21, 23$ ) due to the presence of an unpaired  $1d_{5/2}$  proton an influence of core polarization effects is expected [11]. A large admixture of intruder states of at least 50% has been deduced in order to obtain a better agreement between the experimental  $g$ -factor values and the SDPF-M shell model prediction. In order to reproduce the measured magnetic moment of  $^{34}\text{Al}$ , mixed configurations involving the  $1d_{5/2}$  proton were also assumed. A significant improvement was achieved by using a modified version of the SDPF-M interaction with an  $N = 28$  gap modified to reproduce the excitation energy of the  $3/2^-$  state in  $^{35}\text{Si}$  [12,18]. As a consequence, the energy of the  $2p_{3/2}$  orbital was decreased by 0.5 MeV with respect to the original *sd**f* orbital. Recently, the discovery of the shape coexisting  $0^+$  state in  $^{32}\text{Mg}$  at 1058 keV by a two-neutron transfer reaction has underlined how the SDPF-M effective interaction underestimates the  $p_{3/2}$  component in the  $^{32}\text{Mg}$  ground-state wave function [19]. Only  $\beta$ -decay studies have been done at  $Z = 13$  and  $N = 22, 23$ . Information on the  $^{35}\text{Al}$  excited states is missing. Shell model calculations predict for the  $^{36}\text{Al}$  ground state a value  $I^\pi = 4^-$ , as in  $^{34}\text{Al}$ . New experimental inputs are therefore needed.

Single-neutron removal reactions in inverse kinematics with heavy ions at high energies are known to provide specific information on the single-particle occupancy and correlation effects in nuclei, especially toward the drip lines (see reviews [4,20,21]). In order to study the single-particle mixing for  $N = 20$  to 22 in the Al isotopes, we measured the longitudinal momentum distributions of the  $^{32,33,34,35}\text{Al}$  fragments from one-neutron removal reactions at around 900 MeV/u and the corresponding cross sections. The momentum distribution analysis has been performed in the eikonal framework.

This paper is organized as follows: in Sec. II the experimental method and our data are presented; the momentum distribution analysis is described in Sec. III, where the results are compared with the theoretical model; the inferred single-particle neutron occupancies are given in Sec. IV; conclusions are summarized in the last section.

## II. EXPERIMENTAL TECHNIQUE AND RESULTS

The experiment was performed at the Fragment Separator (FRS) [22] of GSI (Darmstadt). The  $^{33-36}\text{Al}$  beams have been produced in flight via projectile fragmentation of a  $^{48}\text{Ca}$  beam at 1 GeV/u interacting with a Be target ( $6.35 \text{ g/cm}^2$ ) placed at the entrance of the separator. The one-neutron removal reaction data have been extracted from two different FRS settings optimized for the  $^{34}\text{Al}$  and  $^{33}\text{Mg}$  beams. A rate of about 100 ions/s was obtained for the heaviest studied Al isotope (i.e.,  $^{36}\text{Al}$ ), at a primary beam intensity of about  $10^9$  ions/spill.

The experimental setup was the same as described in Ref. [23]. The magnetic rigidity of the separator was set to accept and transmit the ions of interest. The fragment beams were separated and identified up to the midfocal plane F2 where a C reaction target ( $4.05 \text{ g/cm}^2$ ) was located. Particle identification was achieved by using precise tracking detectors (time projection chamber) set in front of and behind the target, as well as at the final focus F4, together with the other standard FRS detectors; multisampling ion chambers (MUSIC) and plastic scintillators, used for the energy-loss and time-of-flight measurements, respectively. Their combined information allows ion identification event by event as well as the measurement of the ion momenta at F4. The particle identification plot at the target position for the  $^{34}\text{Al}$  setting is shown in the top panel of Fig. 1. In the bottom panel of Fig. 1, the identified fragments arriving at F4 and produced after the reaction of  $^{34}\text{Al}$  beams in the C target are plotted. Charge and mass resolutions around  $0.1e$  and  $0.3 \text{ amu}$  were achieved, respectively.

Due to the high-resolution achromatic mode of the FRS, precise momentum measurements ( $\Delta p/p \approx 1.5 \times 10^{-4}$ ) of the produced fragments have been obtained independently of the large momentum spread due to the reactions in the Be target. The momentum of the particle with charge state  $q$  behind the F2 target has been obtained by measuring its position at  $x_{F2}$  and  $x_{F4}$  according to the following equation:

$$p_{\text{lab}} = B\rho q \left( 1 + \frac{x_{F4} - Cx_{F2}}{D_{F2-F4}} \right), \quad (1)$$

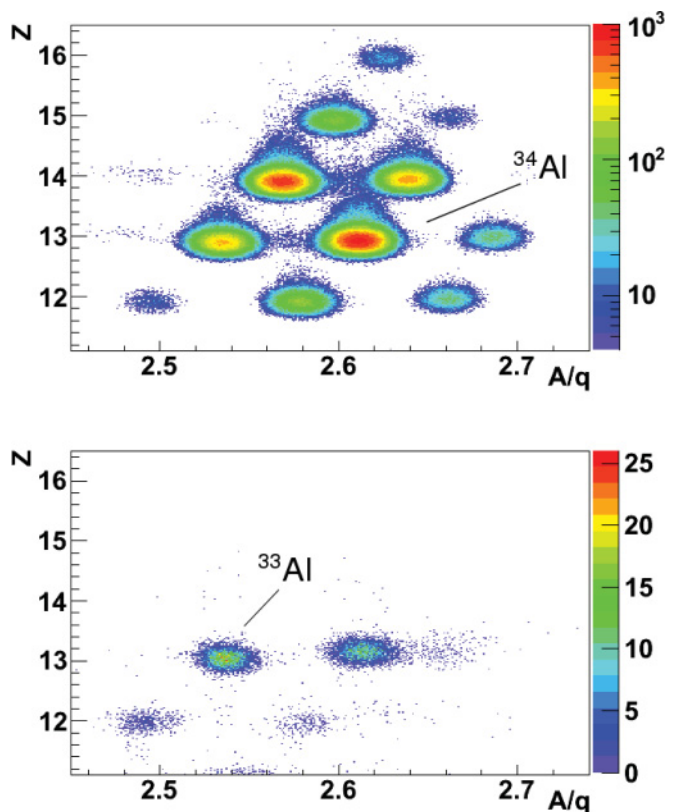


FIG. 1. (Color online) (top panel) Particle identification plot of ion beams at F2 for  $^{34}\text{Al}$  setting. (bottom panel) Particle identification plot of reaction products at F4 for  $^{34}\text{Al}$  events gated at F2.

where  $B\rho$  is the magnetic rigidity of the second half of the FRS (F2-F4) and  $D_{F2-F4}$  is the corresponding dispersion. The coefficient  $C$  includes the optical magnification and corrects for the additional momentum spread due to the presence of matter at F1 and F2. This term has been estimated from the correlation between the two focal plane positions  $x_{F4}$  and  $x_{F2}$ . The longitudinal momentum distribution in the projectile rest frame is given by the Lorentz transformation

$$p_{||} = \gamma (p_{\text{lab}} - \beta E), \quad (2)$$

with  $\beta$  equal to the velocity of the primary fragments,  $\gamma$  being the corresponding Lorentz factor,  $E = \sqrt{p_{\text{lab}}^2 + m^2}$  being the energy of the residual fragment, and  $m$  being its mass.

Due to the high energy of the incoming beams the fragments are scattered to very forward angles (a few mrad) with velocities near that of the corresponding projectile. The detection efficiency for all reaction settings was almost equal to unity. Uncertainty in the cross-section measurements is caused by the background contribution coming from interactions with material in the path of the beam, such as detectors, air, vacuum windows, etc. This was accounted for by background measurements made without the reaction target. For each setting, the background contribution was measured by transmitting the  $(A - 1)$  fragments to F4 without the reaction target at F2. The number of background counts was normalized to the number of incoming fragments at the F2 target and then subtracted from the number of residual fragments detected at F4 with the reaction target inserted. The background measured was about 20%. A comparison of longitudinal momentum distributions measured with and without the target is shown in Fig. 2 for  $^{33}\text{Al}$ . The noninteracting settings were also used as resolution measurements for obtaining the spectrometer function for later convolution with the theoretical distributions. The momentum distribution in the center-of-mass system for the one-neutron removal reaction in  $^{36}\text{Al}$  is shown in Fig. 3 as full points and compared with the resolution (empty points) and the acceptance (dashed lines) of the setup.

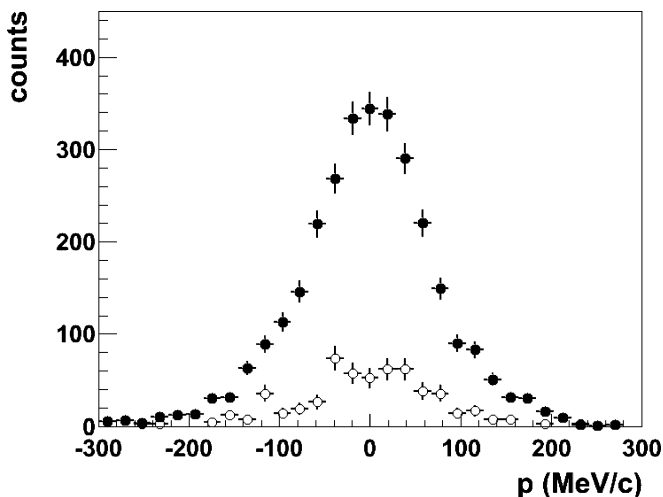


FIG. 2. Measured  $^{32}\text{Al}$  momentum distribution with (full points) and without (empty points) the C target. The error bars represent statistical contributions. Both data sets are normalized to the same number of incoming  $^{33}\text{Al}$  ions.

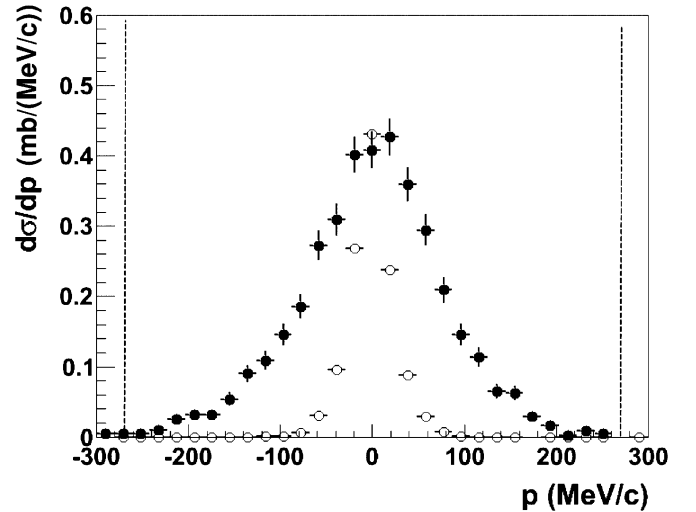


FIG. 3. Measured  $^{35}\text{Al}$  momentum distribution (full points) and the noninteracting  $^{36}\text{Al}$  beam (empty points) with target. The error bars include statistical contributions. The momentum resolution at F4 is normalized to the maximum. The dashed lines represent the full momentum acceptance.

To obtain a proper value for the one-neutron removal cross section we have also corrected the number of the incoming projectiles measured in front of the reaction target and the number of the detected residual fragments at F4 for losses. Losses in the detector material and air, transmission losses between F2 and F4, and detection efficiency have been taken into account to obtain the correct number of fragments coming out of the F2 target. The absorption in the C target, both for the numbers of incoming projectiles  $A$  and fragments  $(A - 1)$ , has been estimated (about 13%) and taken into account.

The transmission losses between F2 and F4 were estimated with the MOCADI code [24] for each setting. A constant transmission throughout the setup has been achieved by restriction of the phase space of the incoming fragments. Further phase-space restrictions did not change the calculated cross sections within the statistical uncertainties. A systematic error comes from the uncertainty of the total transmission (below 4%). Another systematic error is due to thickness uncertainty of the reaction target (about 1%). The measured one-neutron removal cross sections  $\sigma_{-1n}$  of  $^{33,34,35,36}\text{Al}$  with their total errors are listed in Table I.

Since the measured momentum distributions of the residues do not have a Gaussian shape, to evaluate their full width at half maximum (FWHM) we fit the measured data with the following function:

$$f(x) = \begin{cases} p_1 \exp\left(\frac{p_4^2(2x-2p_2+p_4^2)}{2p_3^2}\right) & \text{if } x < p_2 - p_4^2 \\ p_1 \exp\left(\frac{(x-p_2)^2}{2p_3^2}\right) & \text{if } x \in (p_2 - p_4^2, p_2 + p_5^2) \\ p_1 \exp\left(\frac{p_5^2(2x-2p_2+p_5^2)}{2p_3^2}\right) & \text{if } x > p_2 + p_5^2, \end{cases} \quad (3)$$

where  $p_1$  to  $p_5$  are fit parameters. The fit FWHMs corrected for the spectrometer function by subtracting the squared values are given in Table I.

TABLE I. Measured one-neutron removal cross sections  $\sigma_{-1n}$  and widths (FWHM) of the momentum distributions of Al isotopes.

	$I_{gs}^{\pi}$	$E$ (MeV/u) <sup>a</sup>	$\sigma_{-1n}$ (mb)	FWHM (MeV/c)	$\sigma_{-1n}$ (mb) <sup>b</sup>
<sup>33</sup> Al	5/2 <sup>+</sup>	922	64 ± 3	136 ± 3	
<sup>34</sup> Al	4 <sup>-</sup>	880	81 ± 4	134 ± 3	102 ± 24
<sup>35</sup> Al	5/2 <sup>+</sup>	916	75 ± 4	145 ± 3	65 ± 18
<sup>36</sup> Al	(4 <sup>-</sup> )	877	95 ± 5	140 ± 3	

<sup>a</sup>At the middle of the target.

<sup>b</sup>See Ref. [25].

In the last column of Table I the previous cross-section measurements found in the literature are also listed. Our cross sections agree with the values given in Ref. [25] for <sup>34,35</sup>Al and have smaller uncertainties.

### III. MOMENTUM DISTRIBUTION ANALYSIS

Before to going into the details of the analysis of the experimental data we point to an important difference between the odd- and even-mass Al isotopes. The odd-mass isotopes can be well understood in terms of a proton single-particle state coupled to a Mg core of mass number  $A - 1$ . The even-mass Al isotopes, however, are described more appropriately as a proton-particle neutron-hole configuration with respect to a Mg core of the same mass number  $A$ . In the first case, neutron removal reactions will preferentially test the neutron single-particle shell structure. Removal from the core excited components of the ground-state wave function may occur, leaving the residual nucleus in a core excited state. However, such a process will contribute only significantly to the cross section if the core excited configuration carries large fraction of the spectroscopic strength. In the second case, when  $A$  is an even number, the situation is such that the unpaired proton and neutron will interact through the isovector particle-hole interaction leading to Landau damping and random-phase-approximation-type (RPA-type) particle-hole correlations. Thus, removal reactions on odd-mass and even-mass Al isotopes will test different aspects of nuclear dynamics. In the data analysis we have taken care of those differences.

To perform the momentum analysis of our one-neutron removal momentum distributions we make use of the eikonal approximation, well suitable at relativistic energies. The MOMDIS code [26] has been adopted to calculate the theoretical momentum distributions. The wave functions of the bound states have been calculated in a Woods-Saxon potential with reduced radius parameter  $r_0 = 1.25$  fm and diffuseness  $a = 0.7$  fm. No spin-orbit term has been considered. The depth of the well was obtained by reproducing experimental one-neutron separation energies. In the  $S$ -matrix calculations, the target density distribution has been calculated in a modified harmonic oscillator potential to reproduce the radius  $R = 2.31$  fm of the <sup>12</sup>C nucleus [27]. For the core densities two-parameter Fermi functions have been used, reproducing the radius values extrapolated from Na and Mg interaction-cross-section data [28].

We calculate the single-particle cross section  $\sigma^{\text{sp}}$  as the sum of two contributions; for example,  $\sigma_{\text{stri}}^{\text{sp}} + \sigma_{\text{diff}}^{\text{sp}}$ , according to Ref. [29]. The Coulomb breakup contribution was assumed

to be small owing to the light target. The cross sections are calculated in terms of  $S$ -matrices of the core-target and nucleon-target system, expressed as functions of the impact parameters, and the nucleon-core relative motion wave function, calculated by solving the Schrödinger equation for bound states. Comparing the measured longitudinal momentum distribution of the residual fragment with the theoretical one, we deduce information on the orbital angular momentum of the knocked-out neutron and thus on the single-particle ground state of the studied nuclei.

The inclusive momentum distributions and cross sections have been analyzed with the condition that the final states reached in the residual fragments are below the one-neutron separation energy. The experimental energies of the core states with their spins and parities have been considered. Whenever they are not well known, different choices, mentioned in the text, have been used. Since our data include both core emitted in the ground or excited state, we have calculated the momentum distributions for different  $l$  components, where  $l$  is the orbital angular momentum of the removed neutron. We approximate the wave function of the broken-up system as the wave functions of residual fragment (or core) and nucleon. For the Al nucleus of mass number  $A$  the one-neutron removal cross section can be written as the sum of the single-particle cross sections  $\sigma^{\text{sp}}[\psi_{nlj} \otimes \text{Al}(I_c^{\pi})]$  calculated for the neutron plus  $(A - 1)$  core configurations, where  $\psi_{nlj}$  represents the single-particle component in the ground-state wave function of the nucleus  $A$  and  $I_c$  indicates the spin and parity of the Al core with mass number  $(A - 1)$ :

$$\sigma_{-1n} = \sum_l S_l \sigma^{\text{sp}}[\psi_{nlj} \otimes \text{Al}(I_c^{\pi})]. \quad (4)$$

Each coefficient  $S_l$  of Eq. (4) is related to the  $l$  neutron occupation probability in the nucleus and can be compared to the spectroscopic factors calculated by shell model calculations. For <sup>33</sup>Al, the shell model calculations in the  $sd$  space using the USDB interaction has been used [30]. For  $N = 21, 22$  we have used the results of shell model calculations performed in the  $sdpf$  space found in Refs. [10,12]. Due to the lack of spectroscopic, theoretical, and experimental information on <sup>36</sup>Al, it was not possible to compare the data with any theoretical predictions.

Before the comparison with the data, each theoretical momentum distribution was convoluted with the instrumental response. The coefficients  $S_l$  are found from a best-fit  $\chi$ -square minimization to the data.

TABLE II. Calculated spectroscopic factors  $C^2S$ , theoretical single-particle cross sections  $\sigma^{\text{sp}}$ , fit parameters  $S_I$  and experimental cross sections  $\sigma_{-1n}$  for different single-particle states of Al isotopes [ $\psi_{nlj} \otimes Al(I_c^{\pi})$ ].

Isotopes	$\psi_{nlj}$	$I_c^{\pi}$	$E$ (MeV)	$C^2S$	$\sigma^{\text{sp}}$ (mb)	$S_I$	$\sigma_{-1n}$ (mb)
<sup>33</sup> Al							
$l = 0$	1/2 <sup>+</sup>	2 <sup>+</sup> <sup>a</sup>	0.657	0.05	28.6	0.93 <sup>+0.28</sup> <sub>-0.13</sub>	26.4 <sup>+8.0</sup> <sub>-3.7</sub>
	1/2 <sup>+</sup>	(2 <sup>+</sup> ) <sup>b</sup>	0.735		28.4		
	1/2 <sup>+</sup>	3 <sup>+</sup> <sup>a</sup>	1.774	0.49	25.9		
	1/2 <sup>+</sup>	3 <sup>+</sup> <sup>a</sup>	2.360	0.43	24.7		
	1/2 <sup>+</sup>	2 <sup>+</sup> <sup>a</sup>	2.392	0.41	24.6		
	1/2 <sup>+</sup>	2 <sup>+</sup> <sup>a</sup>	3.802	0.02	22.3		
$l = 2$	5/2 <sup>+</sup>	1 <sup>+</sup>	0	0.02	21.4	1.73 <sup>+0.27</sup> <sub>-0.15</sub>	37.0 <sup>+3.2</sup> <sub>-7.6</sub>
	5/2 <sup>+</sup>	3 <sup>+</sup> <sup>b</sup>	1.774	0.03	19.0		
	5/2 <sup>+</sup>	1 <sup>+</sup> <sup>a</sup>	2.765		17.9		
	3/2 <sup>+</sup>	1 <sup>+</sup>	0	0.44	21.4		
	3/2 <sup>+</sup>	4 <sup>+</sup> <sup>b</sup>	0.543	1.44	20.5		
	3/2 <sup>+</sup>	2 <sup>+</sup> <sup>b</sup>	0.657	0.67	20.4		
	3/2 <sup>+</sup>	(2 <sup>+</sup> ) <sup>a</sup>	0.735		20.3		
	3/2 <sup>+</sup>	(4 <sup>+</sup> ) <sup>a</sup>	0.957		20.0		
	3/2 <sup>+</sup>	3 <sup>+</sup> <sup>b</sup>	1.774	0.54	19.0		
	3/2 <sup>+</sup>	3 <sup>+</sup> <sup>b</sup>	2.360	0.42	18.4		
	3/2 <sup>+</sup>	2 <sup>+</sup> <sup>b</sup>	2.392	0.05	18.3		
	3/2 <sup>+</sup>	1 <sup>+</sup> <sup>a</sup>	2.765		17.9		
	3/2 <sup>+</sup>	1 <sup>+</sup> <sup>a</sup>	3.201		17.5		
	$l = 1$	3/2 <sup>-</sup>	(4 <sup>-</sup> ) <sup>a</sup>	1.178			
$l = 3$	7/2 <sup>-</sup>	(4 <sup>-</sup> ) <sup>a</sup>	1.178		19.9	<0.38	<7.6
<sup>34</sup> Al							
$l = 3$	7/2 <sup>-</sup>	5/2 <sup>+</sup>	0		24.3	<0.6	<11.0
	7/2 <sup>-</sup>	5/2 <sup>+</sup> <sup>c</sup>	0.730		22.9		
	7/2 <sup>-</sup>	5/2 <sup>+</sup> <sup>d</sup>	1.618		21.6		
	7/2 <sup>-</sup>	(1/2 <sup>+</sup> ) <sup>e</sup>	3.714		19.2		
	7/2 <sup>-</sup>	(3/2 <sup>+</sup> ) <sup>e</sup>	4.730		18.3		
$l = 1$	3/2 <sup>-</sup>	5/2 <sup>+</sup>	0		47.1	0.97 <sup>+0.10</sup> <sub>-0.45</sub>	45.7 <sup>+4.7</sup> <sub>-26.4</sub>
	3/2 <sup>-</sup>	5/2 <sup>+</sup> <sup>c</sup>	0.730		41.8		
	3/2 <sup>-</sup>	(5/2 <sup>+</sup> ) <sup>e</sup>	1.618		37.2		
$l = 2$	5/2, 3/2 <sup>+</sup>	(7/2 <sup>-</sup> ) <sup>e</sup>	3.714		19.1	1.40 <sup>+0.63</sup> <sub>-0.58</sub>	26.7 <sup>+12.1</sup> <sub>-11.0</sub>
	5/2 <sup>+</sup>	(3/2 <sup>-</sup> ) <sup>e</sup>	4.730		18.0		
$l = 0$	1/2 <sup>+</sup>	(7/2 <sup>-</sup> ) <sup>e</sup>	3.714		27.0	<1.45	<39.2
<sup>35</sup> Al							
$l = 3$	7/2 <sup>-</sup>	4 <sup>-</sup>	0		19.4	1.06 <sup>+0.31</sup> <sub>-0.39</sub>	20.6 <sup>+6.0</sup> <sub>-8.1</sub>
	7/2 <sup>-</sup>	(4 <sup>-</sup> ) <sup>f</sup>	0.657		18.7		
$l = 1$	3/2 <sup>-</sup>	4 <sup>-</sup>	0		31.8	0.59 <sup>+1.15</sup> <sub>-0.59</sub>	18.8 <sup>+36.5</sup> <sub>-18.8</sub>
	3/2 <sup>-</sup>	(4 <sup>-</sup> ) <sup>f</sup>	0.657		29.9		
$l = 2$	5/2, 3/2 <sup>+</sup>	(1 <sup>+</sup> ) <sup>g</sup>	0.200		19.5	0.63 <sup>+0.14</sup> <sub>-0.28</sub>	12.3 <sup>+2.7</sup> <sub>-5.5</sub>
	5/2, 3/2 <sup>+</sup>	(2 <sup>+</sup> ) <sup>g</sup>	0.800		18.4		
$l = 0$	1/2 <sup>+</sup>	(2 <sup>+</sup> ) <sup>g</sup>	0.800		26.1	0.89 <sup>+0.58</sup> <sub>-0.89</sub>	23.2 <sup>+38.4</sup> <sub>-23.2</sub>

<sup>a</sup>USDB calculation.<sup>b</sup>Reference [13].<sup>c</sup>Reference [14].<sup>d</sup>Reference [11].<sup>e</sup>Reference [10].<sup>f</sup>Reference [33].<sup>g</sup>Reference [12].

### A. $^{33}\text{Al}$ results

According to  $sd$  shell model predictions in the ground state of  $^{33}\text{Al}$  ( $S_n = 5.54$  MeV [31]), the  $s$  and  $d$  orbitals are fully occupied (shell closure). Also, our own Hartree-Fock-Bogoliubov (HFB) calculations predict a perfect closure of the  $N = 20$  shell. The  $1d_{3/2}$  orbital is the valence level. The  $1f_{7/2}$  neutron orbital is already bound, while the states of the  $2p$  shell are still unbound. A sharp  $3/2^-$  resonance is found at only 40 keV above threshold. Thus, from the HFB level structure, we expect that the removal cross section is determined by  $sd$ -shell contribution with a preference of  $d_{3/2}$  removal. However, if interactions beyond mean field are present, the picture will change. In particular, the  $3/2^-$  response might be lowered into the bound-state region by core polarization or  $NN$  correlations of another type.

The spin and parity of the ground state is assumed to be  $I^\pi = 5/2^+$  due to the unpaired proton. The known core excited states are taken from Ref. [13]. All allowed core-neutron configurations having a neutron with orbital angular momentum  $l = 0$  to 3 compatible with experimental results are listed in Table II. The corresponding single-particle cross sections, calculated for spectroscopic factor equal to one are listed in the same Table II. The theoretical wave function configurations having a neutron with orbital angular momentum  $l = 0, 2$ , obtained using the calculated USDB single-particle energies, and the associated cross sections are also shown for comparison. Some discrepancies between the theoretical and experimental energy spectra of  $^{32}\text{Al}$  are present at low excitation energy, similar to those pointed out in Ref. [32]. The theoretical spectroscopic factors for the  $2s_{1/2} \otimes ^{32}\text{Al}(2^+, 3^+)$  and  $1d_{3/2} \otimes ^{32}\text{Al}(1^+, 2^+, 3^+, 4^+)$  configurations are  $C^2S = 1.40$  and  $C^2S = 3.61$ , respectively.

In Fig. 4 the measured experimental momentum distribution of  $^{32}\text{Al}$  fragments is represented by the points. The attempt

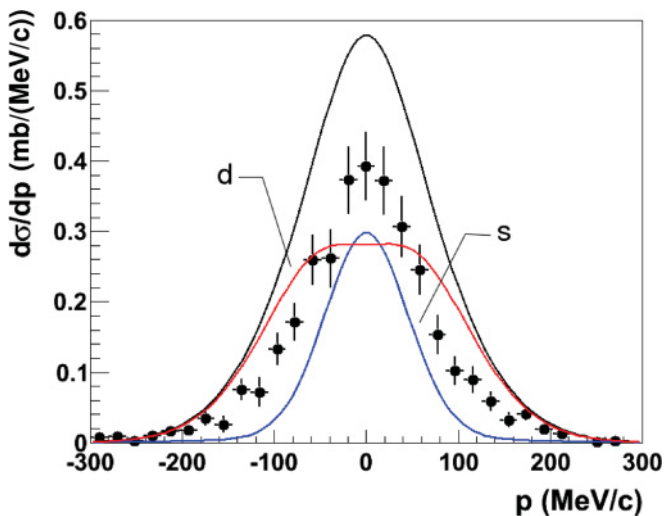


FIG. 4. (Color online)  $^{32}\text{Al}$  momentum distribution: experimental data are shown as full points; error bars include statistical and systematic contributions. The lines labeled  $s$  and  $d$  are the USDB momentum distributions calculated for  $l = 0$  and  $l = 2$  orbital angular momenta, respectively, according to Table II. The full line represents the result of the summed  $l = 0$  and  $l = 2$  contributions.

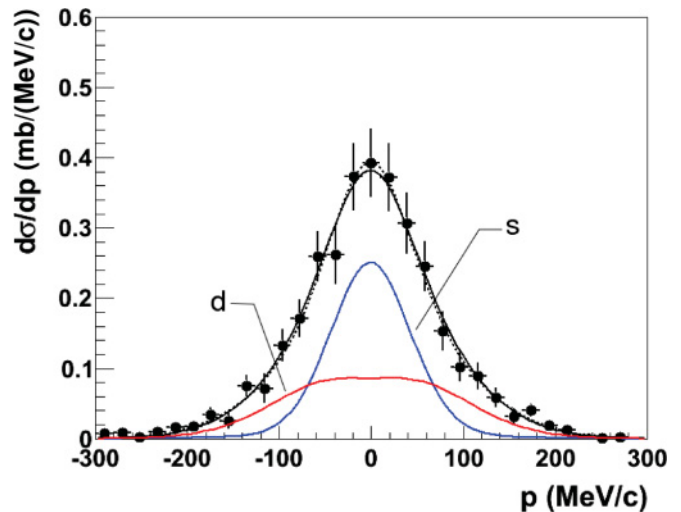


FIG. 5. (Color online)  $^{32}\text{Al}$  momentum distribution: experimental data are shown as full points; error bars include statistical and systematic contributions. The full line represents the result of the fit assuming  $l = 0$  and  $l = 2$  contributions. The lines labeled  $s$  and  $d$  are the momentum distributions calculated assuming  $l = 0$  and  $l = 2$  orbital angular momenta, respectively, for a spectroscopic factor equal to one. The dotted line is the result of a calculation obtained including the excited core configuration  $^{32}\text{Al}(1^+, 3.201$  MeV).

to reproduce the momentum distribution data assuming the USDB single-particle energies and spectroscopic factors is shown in Fig. 4. The USDB momentum distributions calculated assuming  $l = 0, 2$  are indicated with  $s$  and  $d$ , respectively. Their sum plotted as a full line clearly overestimates the data distribution.

The second attempt in describing the data consists in selecting the momentum distribution assuming  $l = 0, 2$  calculated for the lowest experimental energy of the core. They are plotted for a spectroscopic factor equal to one in Fig. 5. The coefficients extracted by fitting the data are  $S_0 = 0.93 \pm 0.13$  and  $S_2 = 1.73 \pm 0.15$ . Systematic uncertainties are included in the errors. The result of the fit is plotted as a full line in Fig. 5. Changes of the momentum distribution calculated for  $l = 2$  and  $2^+$  and  $4^+$  core state contributions are within the errors (see Table II). The  $s$ - and  $d$ -wave occupation probabilities are about 30% and 50% lower than predicted, respectively. On the other hand, we observe that  $S_0$  increases up to  $1.09 \pm 0.12$  when the distribution obtained for the core state  $1^+$  at  $E = 3.201$  MeV is considered. In this case, the  $s$ -wave occupation probability still differs by at least 14% from that predicted. The curve fit is represented by the dashed line of Fig. 5. Combining the results of the fits we can provide the upper and lower limits for both  $s$ - and  $d$ -wave contributions (i.e.,  $S_0 = 0.93^{+0.28}_{-0.13}$  and  $S_2 = 1.73^{+0.27}_{-0.15}$ ). The corresponding  $\sigma_{-1n}$  cross sections are given in the last column of Table II. In order to assume the neutron knocked out from a  $p$  or  $f$  wave, we have to include a contribution from the negative-parity excited states of  $^{32}\text{Al}$  (e.g., from the upper  $pf$  shell). A state at  $E = 1.178$  MeV was identified in a  $\beta$ -decay measurements of  $^{32}\text{Mg}$  and is indicated as a  $4^-$  state [13]. The calculated momentum distributions for  $l = 1, 3$  at this core energy are plotted in Fig. 6 and indicated

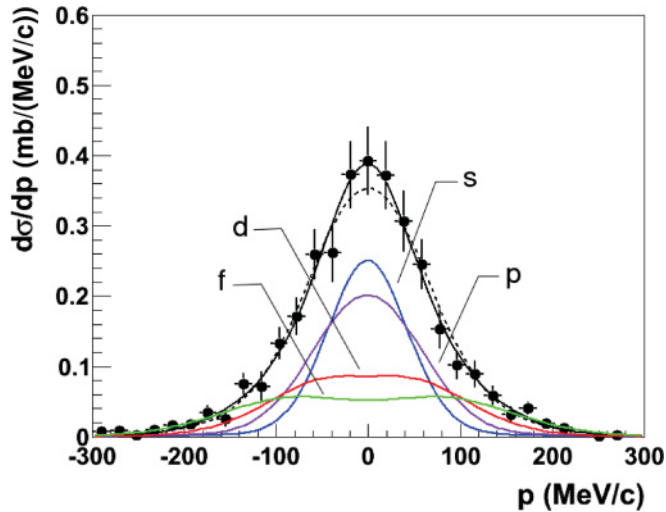


FIG. 6. (Color online)  $^{32}\text{Al}$  momentum distribution: experimental data are shown as full points; error bars include statistical and systematic contributions. The lines labeled  $s$ ,  $p$ ,  $d$ ,  $f$  are the momentum distributions calculated assuming  $l = 0, 1, 2, 3$  orbital angular momentum, respectively, for a spectroscopic factor equal to one. The full line represents the result of the fit including all four  $l$  contributions. The dashed line is the result of a calculation with the coefficient  $S_0 = 0$ .

by  $p$  and  $f$ , respectively, for a spectroscopic factor equal to unity. A fit to the data including all angular orbital terms gives  $S_1 = 0$  and  $S_3 = 0.20 \pm 0.18$ , leaving the  $s$  and  $d$  contributions almost unchanged. The result of this fit is plotted in Fig. 6 as a full line. An upper limit of 12% has been estimated for the  $f$  contribution to the cross section (see Table II). As a consequence the data exclude the presence of intruder states, unless the  $s$  contribution is suppressed.

In order to appreciate a non-negligible presence of intruder configurations in the  $^{33}\text{Al}$  wave function we would need to fix  $S_0 = 0$  in Eq. (4). For completeness, we show the results in describing the  $^{32}\text{Al}$  momentum distribution under this strong assumption. The new fit to the data is plotted in Fig. 6 as a dotted line. The fit  $l = 1$  coefficient provides the upper limit for the  $p$ -wave component (see Table II). Under the hypothesis of a negligible  $s$ -wave occupation probability in the  $^{33}\text{Al}$  wave function, our momentum distribution data would be compatible with the presence of at least 60% intruder states, in agreement with the experimental knowledge on the  $g$  factor and quadrupole moment measurements [11,16]. This possibility meets a scenario where the  $N = 20$  shell closure is broken. Since the data can be well described with only  $l = 0, 2$  contributions and no full  $sdpf$  calculations are at the moment available for a comparison, we do not fully discard an  $s$ -wave component in the  $^{33}\text{Al}$  single-particle wave function.

### B. $^{34}\text{Al}$ results

In  $^{34}\text{Al}$  at least one valence neutron occupies the  $pf$  shell. The spin and parity of the ground state are assigned as  $I^\pi = 4^-$  [12,34–36]. The neutron separation energy is  $S_n = 2.47$  MeV [31]. The excitation energies of the core were taken from Ref. [12]. Monte Carlo shell model calculations predict the

low-lying  $^{33}\text{Al}$  states as intruder states ( $2p-2h$ ) [10,11]. An additional  $^{33}\text{Al}$  state was observed in an inelastic scattering experiment [14] at 730 keV, very close to the predicted one, and interpreted thus as a  $2p-2h$  state of the same spin and parity as the ground state. All possible core-neutron configurations having a neutron with orbital angular momentum  $l = 0$  to 3 and compatible with experimental results are listed in Table II, together with the corresponding calculated single-particle cross sections.

In Fig. 7 the measured experimental momentum distribution of  $^{33}\text{Al}$  fragments is represented by full points. The theoretical momentum distributions calculated for  $l = 0$  to 3 are indicated as  $s$ ,  $p$ ,  $d$ , and  $f$ , respectively, for a spectroscopic factor equal to unity. They have been calculated taking into account the experimentally determined energies of the low-lying core states. No change in the experimental width of the momentum distribution after crossing  $N = 20$  is found compared to the  $^{33}\text{Al}$  data (see Table I). Nevertheless, fitting the distribution with 4 different  $l$  components implies some  $2p_{3/2}$  occupation probability. The reason is due to the different neutron separation energies and the different cross-sections values of the  $p$  components calculated in the two nuclei. The  $l = 1$  fit value is  $S_1 = 0.97^{+0.10}_{-0.45}$ , where the asymmetric errors take into account the configurations with the  $^{33}\text{Al}$  excited states. The  $p$  contribution to the cross section in  $^{34}\text{Al}$  varies between 24% and 62% (see Table II). A contribution to the cross section comes also from the  $d$ -wave component, with  $S_2 = 1.40^{+0.63}_{-0.58}$ , while the coefficients  $S_0$  and  $S_3$  obtained by fitting are about zero. The result of the fit is plotted in Fig. 7 as a full line. Assuming a higher excitation energy of the core does not change the result of the fit because it leads to slightly higher  $s$  contribution. In this case the upper limit of the  $f$  contribution to the cross section is less than 14% (see Table II).

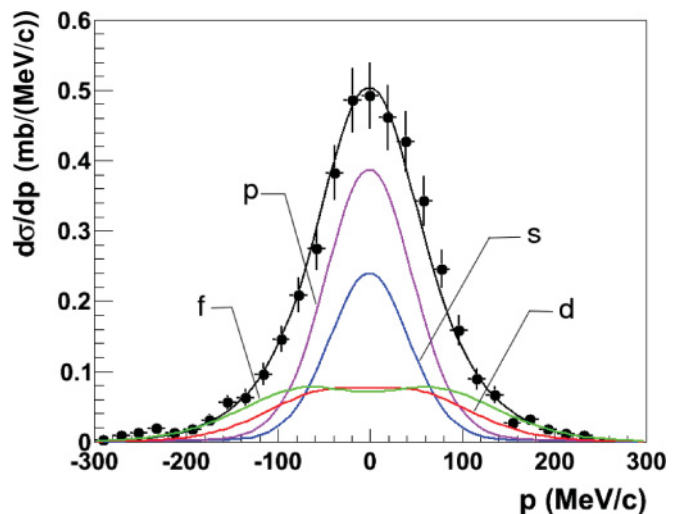


FIG. 7. (Color online)  $^{33}\text{Al}$  momentum distribution: experimental data are shown as full points; error bars include statistical and systematic contributions. The curves labeled  $s$ ,  $p$ ,  $d$ ,  $f$  are the momentum distributions calculated assuming  $l = 0, 1, 2, 3$  orbital angular momentum, respectively, for a spectroscopic factor equal to one. The full line represents the result of the fit including all four  $l$  contributions.

A large spectroscopic strength of the  $2p_{3/2}$  orbital was observed in the  $^{33}\text{Mg}$  nucleus, where lowering of the  $2p_{3/2}$  orbital was needed to reproduce the measured  $^{32}\text{Mg}$  momentum distribution [17]. This may be the reason that a relatively narrow momentum distribution was measured. Thus, the data do not exclude the presence of a  $2p_{3/2}$  level much closer to the  $1d_{5/2}$  than in  $^{33}\text{Al}$ . Under the assumption of a negligible presence of the  $f$  contribution to the momentum distribution, we can make a more quantitative discussion about the  $l = 0$  coefficient. For  $S_3 = 0$ , the  $d$  and  $p$  fit contributions remain unchanged, while the  $s$ -wave contribution to the cross section increases up to a maximum value of 48% (see Table II).

At least 50% of intruder configurations were supposed mixed in the ground state of  $^{34}\text{Al}$  according to Ref. [12]. Our result on the  $2p_{3/2}$  neutron occupancy in the  $^{34}\text{Al}$  ground state and interpretation are in favor of this assumption. Lowering of the energy of the  $2p_{3/2}$  orbital, as suggested in order to reproduce the measured  $g$  factor [12], is thus supported by the measured momentum distribution.

### C. $^{35}\text{Al}$ results

In  $^{35}\text{Al}$  at least two valence neutrons occupy the  $pf$  shell. The spin and parity of the ground state is assumed  $I^\pi = 5/2^+$ , due to the unpaired proton (as for  $^{33}\text{Al}$ ). The neutron separation energy is  $S_n = 5.27$  MeV [31]. Our HFB calculations confirm these expectations. However, they show that the  $sd$  shell closure is partially dissolved, resulting in a slight increase of the  $pf$  shell occupancy by about 9%. Interestingly, without pairing, the  $2p_{3/2}$  orbital is barely bound by only 45 keV. Pairing increases the binding energy to about 5.26 MeV, in almost perfect agreement with the empirical value. Hence, we find an enhancement of valence pairing in this nucleus. The  $2p_{1/2}$  level, however, is not yet bound; that is, the neutron separation energy threshold is located in between the  $2p$ -shell spin-orbit partners. Analyzing the calculated continuum HFB level density, one finds a significant amount of  $s$ -wave strength only at 2.87 MeV, which is much too far from the threshold for being mixed by  $p$ - and  $f$ -wave partial contributions. Hence, from HFB calculations we expect that the removal cross section is given mainly by  $pf$ -wave contributions.

We consider the proton to be a spectator, not contributing to the dynamics of the  $^{35}\text{Al}$  valence sector. However, no experimental  $\gamma$  transitions associated with positive-parity states have been identified below 1 MeV excitation energy in  $^{34}\text{Al}$  [12]. In order to include possible positive-parity states we have considered predictions from shell model calculations performed in the  $pf$  space [12]. Concerning their spin and parity assignment, we have taken into account the results of the SDPF-M calculation shown in Fig. 4 of Ref. [12]. In our calculations we fixed a level at 200 keV with  $I^\pi = 1^+$  and the one at 800 keV with  $I^\pi = 2^+$ . These two states can contribute to the final configurations with  $l = 0$  and  $l = 2$ , as listed in Table II. Among the possible configurations with negative parity states of the core we have included the state identified at about 650 keV in an experiment of Coulomb excitation of  $^{34}\text{Al}$  [33]. This state is considered to be a good candidate for a highly mixed normal intruder state with  $I^\pi = 4^-$ . The

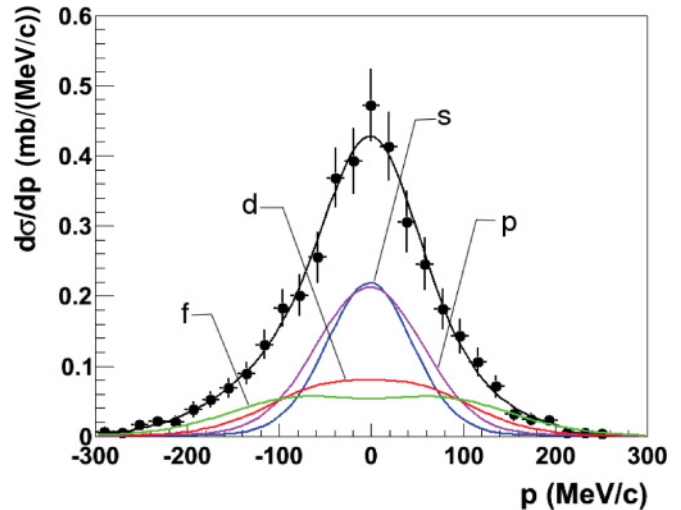


FIG. 8. (Color online)  $^{34}\text{Al}$  momentum distribution: experimental data are shown as full points; error bars include statistical and systematic contributions. The curves labeled  $s$ ,  $p$ ,  $d$ ,  $f$  are the momentum distributions calculated assuming  $l = 0, 1, 2, 3$  orbital angular momentum, respectively, and a spectroscopic factor equal to one. The full line represents the result of the fit including all four  $l$  contributions.

single-particle cross sections have been calculated and listed in Table II for all these core-neutron configurations.

In Fig. 8 the measured momentum distribution of  $^{34}\text{Al}$  fragments is represented by the full points. The theoretical momentum distributions calculated for  $l = 0$  to 3 are shown as  $s$ ,  $p$ ,  $d$ , and  $f$ , respectively, for spectroscopic factors equal to one. They have been calculated for the lowest experimental energy of the core. Similarly to the previous Al systems, only  $s$ - or  $p$ -wave contributions cannot give a good description of the data. Fitting the data with all four  $l$  terms of Eq. (4), we obtain that none of the four terms are negligible, making the data interpretation more difficult. The result of the fit is shown in Fig. 8 as a full line. Different energies of the core do not make a significant change in the values of the fit coefficients. The measured probabilities to remove one neutron from the  $2s_{1/2}$  and  $2p_{3/2}$  orbitals are affected by large errors. We notice that the experimental distribution is less symmetric than in the other studied cases. The reason is mainly due to the presence of larger statistical fluctuations in the background contribution. This is the explanation of large errors of the fit parameters. Beside the restrictions we can provide the upper limit for the  $l = 0$  and  $l = 1$  contributions. As a consequence the coefficients obtained by fitting and taking into account different core energies are  $S_0 = 0.89^{+0.58}_{-0.89}$ ,  $S_1 = 0.59^{+1.15}_{-0.59}$ ,  $S_2 = 0.63^{+0.14}_{-0.28}$ , and  $S_3 = 1.06^{+0.31}_{-0.39}$ . The  $S$  values are listed in Table II together with the corresponding cross sections. The upper limit of the  $s$ -wave contribution to the cross section is 25%. The  $d$  and  $f$  components contribute about 16% and 27%, respectively. On the other hand, the lack of experimental and theoretical knowledge about the studied nucleus prevents a clearer interpretation of its shell structure. We notice that the  $l = 3$  occupancy is higher than in the  $^{34}\text{Al}$  results. The occupation probability for the  $2p_{3/2}$  level becomes

significantly higher if we fix  $S_0 = 0$ . Under the assumption of negligible  $s$ -wave contribution, the neutron would be mostly removed from the  $p$  orbital, with an upper limit of about 31% of the total cross section.

#### IV. OCCUPATION PROBABILITY RESULTS

The results of the momentum distribution analysis in terms of different orbital angular momenta provide information on the evolution of the single particle occupancy in the ground state of the  $^{33,34,35}\text{Al}$ . In Fig. 9, the values of the coefficients  $S_l$  coming from the fit momentum distributions listed in Table II are plotted as a function of the neutron number ( $N = 20$ –22). At  $N = 20$  the USDB shell model scenario predicts the ground-state wave function of the  $^{33}\text{Al}$  interpreted without the presence of intruder states. Our experimental results at  $N = 20$  do not confirm the USDB shell model prediction. The measured  $2s_{1/2}$  neutron occupancy in the  $^{33}\text{Al}$  wave function is 20% to 40% lower than the predicted USDB value. The uncertainty about the core state selection excludes an agreement better than 14%. The predicted and measured  $1d_{3/2}$  neutron occupancy differ by a factor two. The present conclusions are quite different from the one drawn in Ref. [37] for the  $N = 16$  subshell closure. There, it was found that in  $^{23}\text{O}$  ( $S_n = 2.74$  MeV), a system which is dominated by a configuration with a  $l = 0$  valence neutron, a corresponding analysis confirmed the  $s$ -wave strength predicted by the USDB shell model. A limitation in the interpretation of the  $^{33}\text{Al}$  inclusive data within a  $sd$  shell model is clearly found.

We have performed a momentum analysis including  $l = 1$  strength in the Al ground-state wave functions. The single particle  $2p_{3/2}$  occupancy in Al isotopes is non-negligible at  $N = 21$ . At  $N = 22$ , the uncertainty associated to with the  $S_1$  coefficient does not allow to establish this occupancy. The large uncertainty on the  $S_0$  coefficients also prevents definitive conclusions on  $s$  removal probability. Instead, we observe a well-established trend for the  $d$  and  $f$  neutron occupancies. A gradual decrease of the  $1d_{3/2}$  strength is found

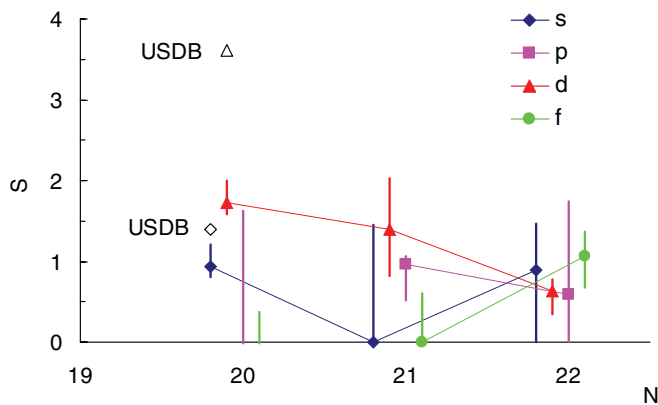


FIG. 9. (Color online) Extracted single-particle neutron occupancy at  $N = 20$  to 22 in Al isotopes for different  $l$  values. The lines without symbols at  $N = 20$  represent the upper limit for  $l = 1$  (left) and  $l = 3$  (right) obtained for  $S_0 = 0$ . For  $^{33}\text{Al}$  the USDB spectroscopic factors are shown for comparison.

from  $N = 20$  to  $N = 22$ . Correspondingly an increase of the  $1f_{7/2}$  occupancy is found, as expected. This is reflected also in the wider momentum distribution at  $N = 22$  compared to  $N = 20$ . In  $^{33}\text{Al}$ , the occupancy of the  $p$  orbital increases strongly only if the probability to remove a neutron from the  $s$  orbital is negligible. On the contrary, the neutron removal probability from the  $l = 1$  orbital is definitely non-negligible in  $^{34}\text{Al}$ . Qualitatively, this effect would reflect a decrease of the energy gap between the  $2p_{3/2}$  and  $1d_{3/2}$  levels at  $N = 20$ . This scenario was also supported in a description of  $^{33}\text{Mg}$  momentum distribution data [17]. However, similar effects could also be obtained by a splitting of the spectroscopic strength into a fragmented multicomponent spectral distribution having components shifted to lower energies. The observation of such a spectral distribution would be an indication for the suppression of mean-field dynamics and the onset of correlation dynamics. In shell model language, such states would be called intruder states. Core polarization may even lower fractional spectral strength from the next higher major shell into the region under investigation. Although calculations for the mass region under scrutiny are not available, results on other stable and neutron-rich nuclei [38–41] indicate that the coupling of single-particle states to collective multiparticle-hole configurations will increase with neutron excess. The  $sd$  and  $sdpf$  shell model may underestimate such collective couplings because of their necessarily limited configuration spaces.

#### V. SUMMARY

The longitudinal momentum distributions and the one-neutron removal cross sections of  $^{33-36}\text{Al}$  at about 900 MeV/u have been measured. A momentum analysis in terms of orbital angular momenta was performed within the eikonal approach. A strong limitation in the interpretation of the  $^{33}\text{Al}$  inclusive data within an  $sd$  shell model is found. The  $^{32}\text{Al}$  momentum distribution analysis has shown that the measured  $2s_{1/2}$  strength is overestimated by the USDB shell model calculation. The contribution of the intruder configurations seems to be not as large as the SDPF-M shell model predicts, except if the decrease of the  $2p_{3/2}$  level energy is associated with a negligible probability that a neutron is knocked out from the  $2s_{1/2}$  orbital, similarly to  $^{33}\text{Mg}$  [17]. On the other hand, the relatively high neutron separation energies of the Al isotopes allow transitions to many bound final levels and a large part of the one-neutron removal cross section leads to excited states of the residues.

From the systematics no large effects are visible in the cross-section values as the neutron number increases. The measured cross-section values follow the typical trend due to odd-even effects. An higher value is observed at  $N = 23$  compared to  $N = 21$ . The widths in  $^{33}\text{Al}$  and  $^{34}\text{Al}$  are comparable but narrower than in  $^{35}\text{Al}$ . For  $N = 21, 22$ , the single particle  $2p_{3/2}$  and  $1f_{7/2}$  neutron occupancies show an increase, as expected. Correspondingly, the  $1d_{3/2}$  strength decreases. In particular,  $^{34}\text{Al}$  results support a non-negligible probability to remove a neutron from the  $p$  orbital. This probability corresponds to an upper limit of 62% of the total cross section.

Since for  $^{36}\text{Al}$  no spectral information is available, we did not include the  $N = 23$  isotope into the analysis of the momentum distributions.

The measurements have indicated the complexities of the spectroscopy in exotic neutron-rich nuclei. It remains a challenge to describe consistently the removal measured cross sections and longitudinal momentum distributions. The most important reasons for the limitations encountered in our analysis are related in large extent to the (incoherent) mixture of various states in the recorded cross sections. Without a high  $\gamma$ -energy resolution tagging allowing to separate removal from the ground and excited states, a detailed and dependable

analysis of the future data beyond the level reached here is probably hard to achieve. Despite these constraints we have added new information on the shell structure around  $N = 20$ .

#### ACKNOWLEDGMENTS

We are indebted to B. A. Brown for providing us the USDB shell model calculations and spectroscopic factors. We are grateful to A. Bonaccorso for fruitful discussions. We acknowledge the excellent support of the FRS technical staff. Support from NSERC, Canada is also gratefully acknowledged.

- 
- [1] E. K. Warburton, J. A. Becker, and B. A. Brown, *Phys. Rev. C* **41**, 1147 (1990).
  - [2] C. Thibault *et al.*, *Phys. Rev. C* **12**, 644 (1975).
  - [3] C. Detraz *et al.*, *Phys. Rev. C* **19**, 164 (1979).
  - [4] A. Gade and T. Glasmacher, *Prog. Part. Nucl. Phys.* **60**, 161 (2008).
  - [5] O. Sorlin and M.-G. Porquet, *Prog. Part. Nucl. Phys.* **61**, 602 (2008).
  - [6] E. Caurier, F. Nowacki, A. Poves, and J. Retamosa, *Phys. Rev. C* **58**, 2033 (1998).
  - [7] T. Otsuka, T. Suzuki, M. Honma, Y. Utsuno, N. Tsunoda, K. Tsukiyama, and M. Hjorth-Jensen, *Phys. Rev. Lett.* **104**, 012501 (2010).
  - [8] O. Tarasov *et al.*, *Phys. Lett. B* **409**, 64 (1997).
  - [9] A. C. Morton *et al.*, *Phys. Lett. B* **544**, 274 (2002).
  - [10] Vandana Tripathi *et al.*, *Phys. Rev. Lett.* **101**, 142504 (2008).
  - [11] P. Himpe *et al.*, *Phys. Lett. B* **643**, 257 (2006).
  - [12] P. Himpe *et al.*, *Phys. Lett. B* **658**, 203 (2008).
  - [13] S. Grevy *et al.*, *Nucl. Phys. A* **734**, 369 (2004).
  - [14] W. Mittig *et al.*, *Eur. Phys. J. A* **15**, 157 (2002).
  - [15] P. Doornenbal *et al.*, *Phys. Rev. Lett.* **103**, 032501 (2009).
  - [16] T. Nagatomo *et al.*, *Eur. Phys. J. A* **42**, 383 (2009).
  - [17] R. Kanungo *et al.*, *Phys. Lett. B* **685**, 253 (2010).
  - [18] S. Nummela *et al.*, *Nucl. Phys. A* **701**, 410c (2002).
  - [19] K. Wimmer *et al.*, *Phys. Rev. Lett.* **105**, 252501 (2010).
  - [20] P. G. Hansen and J. A. Tostevin, *Annu. Rev. Nucl. Part. Sci.* **53**, 219 (2003).
  - [21] T. Aumann, *Eur. Phys. J. A* **26**, 441 (2005).
  - [22] H. Geissel *et al.*, *Nucl. Instr. and Meth. B* **70**, 286 (1992).
  - [23] R. Kanungo *et al.*, *Phys. Rev. Lett.* **102**, 152501 (2009).
  - [24] N. Iwasa *et al.*, *Nucl. Instrum. Methods B* **126**, 284 (1997).
  - [25] C. Rodriguez-Tajes *et al.*, *Phys. Rev. C* **82**, 024305 (2010).
  - [26] C. A. Bertulani and A. Gade, *Comp. Phys. Comm.* **17**, 372 (2006).
  - [27] A. Ozawa *et al.*, *Nucl. Phys. A* **691**, 599 (2001).
  - [28] T. Suzuki *et al.*, *Nucl. Phys. A* **630**, 661 (1998).
  - [29] K. Hencken, G. Bertsch, and H. Esbensen, *Phys. Rev. C* **54**, 3043 (1996).
  - [30] B. A. Brown (private communication).
  - [31] G. Audi *et al.*, *Nucl. Phys. A* **729**, 337 (2003).
  - [32] H. Ueno *et al.*, *Phys. Lett. B* **615**, 186 (2005).
  - [33] B. V. Pritychenko, T. Glasmacher, B. A. Brown, P. D. Cottle, R. W. Ibbotson, K. W. Kemper, and H. Scheit, *Phys. Rev. C* **63**, 047308 (2001).
  - [34] P. Baumann *et al.*, *Phys. Lett. B* **228**, 458 (1989).
  - [35] N. Orr *et al.*, *Phys. Lett. B* **258**, 29 (1991).
  - [36] Y. Utsuno, T. Otsuka, T. Glasmacher, T. Mizusaki, and M. Honma, *Phys. Rev. C* **70**, 044307 (2004).
  - [37] D. Cortina-Gil *et al.*, *Phys. Rev. Lett.* **93**, 062501 (2004).
  - [38] F. J. Eckle *et al.*, *Phys. Rev. C* **39**, 1662 (1989).
  - [39] F. J. Eckle *et al.*, *Nucl. Phys. A* **506**, 159 (1990).
  - [40] N. Vinh-Mau, *Nucl. Phys. A* **592**, 33 (1995).
  - [41] H. Lenske, F. Hofmann, and C. M. Keil, *Prog. Part. Nucl. Phys.* **46**, 187 (2001).